Kinetic Monte Carlo study on the decay of two-dimensional nanostructures: Influence of the activation energy of diffusion on kinetic and morphological properties

Marcos F. Castez and Ezequiel V. Albano
Instituto de Investigaciones Fisicoquímicas Teóricas y Aplicadas (INIFTA), Casilla de Correo 16, Sucursal 4, (1900) La Plata, UNLP, CONICET, Argentina

(Received 18 June 2008; published 5 September 2008)

Surface diffusion-mediated decay of two-dimensional nanostructures is studied by means of a kinetic Monte Carlo model. We consider several possible choices for the activation energies associated with possible diffusion paths, including simple phenomenological models, as well as results provided by the embedded atom model. Numerical results show that kinetic aspects of the evolution are quite sensitive to the activation energy model chosen. In contrast, morphological aspects of the evolution exhibit a similar qualitative behavior, irrespective of the activation energy model considered. It is shown that this common behavior closely agrees with predictions from the continuous theory of surface diffusion-driven interface decay.

DOI: 10.1103/PhysRevE.78.031601 PACS number(s): 81.10.Bk, 02.50.Ey, 81.15.Aa, 81.16.−c

I. INTRODUCTION

The study of the dynamic and the morphological stability of nanostructures evolving by surface diffusion currents has attracted great interest in recent years, both from the theoretical and the experimental points of view [1–16]. In fact, such study is closely related to topics of great relevance in emerging nanotechnology, such as the design of new methods in nanofabrication [17,18] or the problem of nanostructure stability [19]. Surface diffusion currents can be useful to change shapes in the nanoworld, e.g., by using a thermal treatment capable of improving a given nanostructure [20]. That would certainly be a "desirable" consequence of surface diffusion currents. Nevertheless, surface diffusion currents can bring "undesirable" effects, as e.g., if a given built nanostructure becomes thermally unstable and decays in macroscopically short times. Within this context, broad knowledge of the dynamic and morphological properties of nanostructure evolution driven by surface diffusion currents becomes necessary in order to develop strategies capable of enhancing the "positive aspects" of surface diffusion, or, in more specific words, controlling these physical processes for a given nanotechnological application.

Continuous theory of interface evolution mediated by surface diffusion is a well-established topic since the pioneering work by Mullins [21,22] and Herring [23,24]. In fact, nowadays it is widely accepted that this theory provides a physically correct description of surface diffusion-driven interface evolution above the roughening temperature T_R [25]. One of the most important contributions from those early studies is the understanding of the relationship between surface diffusion currents and a geometrical property of the surface: the local curvature. In fact, from a mesoscopic point of view, the surface diffusion flux is proportional to the gradient of the local curvature. Of course, in the derivation of such dependence, there is not only an implicit assumption of smoothness for the surface, as is required by a proper definition of curvature, but also an underlying local equilibrium hypothesis to have well-defined thermodynamic coefficients, such as the surface tension.

Most attention in the literature has been payed to the case of interfaces under the so-called small-slope approximation, which corresponds to the study of patterns exhibiting a small amplitude to wavelength ratio. In particular, during past decades there have been many papers dealing with a Langevin equation, directly obtained by applying Mullins's ideas to the small-slope case [26–28], which reads

$$\frac{\partial h(x,t)}{\partial t} = -K\frac{\partial^4 h}{\partial x^4} + \eta(x,t), \tag{1}$$

where h is a single-valued function that describes the interface, K is a constant proportional to the diffusion coefficient, and η is a Gaussian white noise introduced to capture, to some extent, the stochastic nature of the diffusion process. By performing a simple substitution in the linear equation (1) in the absence of noise, i.e., for $\eta \equiv 0$, one can see that at time t a Fourier mode of the initial interface $A\sin(kx)$ evolves into

$$h(x,t) = A\exp(-Kk^4 t)\sin(kx). \tag{2}$$

Equation (2) is quite interesting because it shows that every Fourier mode performs an exponential decay whose lifetime depends on temperature through the constant K and on the wavelength $\lambda = \frac{2\pi}{k}$. Moreover, Eq. (2) shows that the decay constant is proportional to λ^{-4}, i.e., under the small-slope approximation, the linear theory predicts a fast filtering of high-frequency features of a given interface.

The continuous theory of surface diffusion-driven interface evolution has been considered in the literature mainly under such small-slope approximation, i.e., under the linear regime. This was mostly due to the resultant simplicity of the equations rather than to physical motivations. Nevertheless, recent theoretical and simulational work [29,30], where a vectorial, stochastic difference equation for the evolution of two-dimensional interfaces has been considered, has shown that for interfaces that depart from the small-slope approximation, strong deviations from linear theory expectations can be observed. On the one hand, there are differences from a kinetic point of view since at the initial stage a nonexponential decay of interface corrugation was found. On the other hand, there is a transient stage that exhibits a new morphological behavior, because an initially sinelike interface devel-

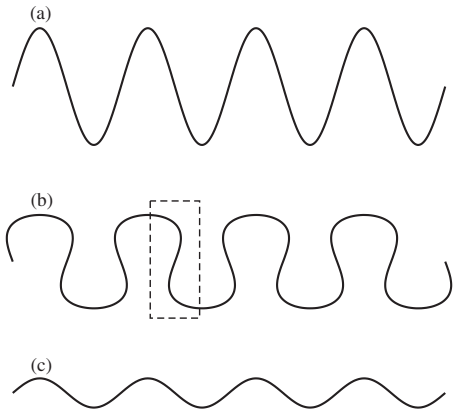

FIG. 1. Schematic view of the decay of sine waves driven by (curvature-dependent) surface diffusion currents in dimension 1+1. In (a) the initial profile, a sine wave far from the small-slope approximation, is shown. (b) represents the transient regime in which the interface develops overhangs spontaneously (as is stressed in the dashed box) and departs from the sinelike shape. Finally, in the late evolution stage, the interface recovers the sinelike shape with a smaller amplitude, as is shown in (c).

ops overhangs spontaneously, and subsequently it recovers the sinelike shape at the final stage of the dynamic evolution. The different stages in the surface diffusion-mediated decaying of high-amplitude sinelike patterns are outlined in Fig. 1. Moreover, as has been pointed out in a recent paper [31], the actual evolution of an initially sinelike pattern far from the small-slope approximation can very closely be approximated by the following vectorial parametric equation:

$$\vec{r}(p,t) = \left(p - B(t)\sin\left(\frac{4\pi p}{\lambda}\right), A(t)\sin\left(\frac{2\pi p}{\lambda}\right)\right), \qquad (3)$$

where $\vec{r}$ is a vectorial function whose value, at a fixed time t, depends only on the parameter p, while $A(t)$ and $B(t)$ are coefficients to be fitted from the numerical data.

Within this scenario, in this paper we present a kinetic Monte Carlo (KMC) model for the study of kinetic and morphological properties of the decay of initially far-from-equilibrium periodic patterns in two dimensions. In particular, we explore several different models for activation energies of diffusion events, comparing the obtained results among the different models, as well as with expectations from the continuous theory.

The rest of the paper is organized as follows: in Sec. II we describe the kinetic Monte Carlo model, its implementation issues, and we introduce the different models for activation barriers that will be considered throughout this work. In Sec. III we present and discuss numerical results concerning kinetic aspects of small aspect-ratio wave decay. Morphological aspects in the case of high aspect-ratio interface evolution are presented in Sec. IV. Finally, in Sec. V we present a summary and the concluding remarks.

II. DESCRIPTION OF THE MODELS

Let us consider a two-dimensional triangular lattice of sides $L_x \times L_y$ on which particles (atoms or molecules) can diffuse. Each site of the lattice can be in one of two possible states: occupied (by a particle) or empty. We shall introduce the occupation number n_{ij} that takes the value 1 if the site (i,j) is occupied and 0 if the site (i,j) is empty. A periodic boundary condition is imposed on the lattice along the x direction, while a free boundary condition is imposed along the y direction by introducing two extra rows in the lattice, corresponding to $j=0$ and $j=L_y+1$, which we shall call the *bottom* and the *top* of the system, respectively. Such extra rows cannot be occupied by particles, and sites on these rows will be called "forbidden sites." We shall assume that every particle on the lattice interacts with its neighbors through the following Hamiltonian:

$$H = E_b \sum_{\langle i,j,l,m \rangle} n_{ij} n_{lm} + 2E_b \sum_{i=1}^{L_x} n_{i1}, \qquad (4)$$

where $\langle\ \rangle$ denotes a nearest neighbor restricted summation and E_b is the bond energy between two nearest neighbor particles. In this way, the first summation corresponds to bulk interactions among particles, while the second one accounts for the interaction between particles and the bottom wall.

In a single diffusion event a particle in the (i,j) position $(1 \leqslant i \leqslant L_x,\ 1 \leqslant j \leqslant L_y)$ of such lattice can jump into one of its six neighboring sites, provided that such site is empty, and, since surface diffusion is the only process considered by the model, the dynamics of the system is conservative and the total number of particles N_T is constant during the whole evolution.

Diffusion processes have been implemented under the KMC approach, with transition rates evaluated according to the harmonic transition state theory, i.e., the transition rate for a transition from configuration c_{ini} to configuration c_{fin} is given by

$$W(c_{ini} \rightarrow c_{fin}) = \nu_0 \exp[-E^{act}(c_{ini}, c_{fin})/k_B T], \qquad (5)$$

where ν_0 is the effective vibration frequency, $E^{act}(c_{ini}, c_{fin})$ is the activation energy for a transition between c_{ini} and c_{fin}, k_B is the Boltzmann constant, and T the absolute temperature. Throughout this work we take $\nu_0 = 5 \times 10^{12}$ Hz. As was pointed out by Weinberg and co-workers [32–34], the kind of dynamics that induces the transition rate given by Eq. (5) satisfies the detailed balance condition for a Boltzmannian equilibrium state as the standard dynamic rules, such as Kawasaki, Glauber, or Metropolis dynamics do [35–38]. Also, $W(c_{ini} \rightarrow c_{fin})$ represents a physical quantity since it is proportional to the probability of success for thermally activated barrier crossing.

A single main loop in the kinetic Monte Carlo model can be summarized as follows:

(1) All possible transitions in the system, involving diffusion events from an occupied site into any unoccupied next neighbor site, are identified and their corresponding transition rates are computed.

(2) A diffusion event is determined by randomly choosing from all the possible jumps weighted by their relative rate of occurrence given by Eq. (5).

(3) The transition is performed and the system is updated.

The Monte Carlo steps (MCS) time unit is defined such that N_T iterations of the preceding loop correspond to one MCS. In the kinetic Monte Carlo approach the connection between "real time" and MCS time is established in the following way: Let μ be a label for all possible transition events in the system. The transition rate $P_\mu = \nu_0 \exp(-\frac{E_\mu}{k_b T})$ has the dimension of a frequency, and its reciprocal can be considered as the residence time for the particle involved in the transition. As transition probabilities for all possible events are independent, the overall probability per unit time for the system to perform a transition is obtained by adding all possible transition rates, namely, $P = \Sigma_\mu P_\mu$. Therefore, $\frac{1}{P}$ is the mean residence time for the system in a specific state and, consequently, it represents the mean time associated with one iteration.

In this work we considered five different models for activation energies. The common feature in all these models is that the activation energy for a transition from the state c_{ini} to the state c_{fin} only depends on the energies of those states. We label these different activation energy models with the acronyms MARM, EINI, EINI-C, EAM-Ni, and EAM-Cu, and these models are described as follows:

(1) MARM: In this model, a harmonic dependence of the energy as a function of the reaction degree is assumed. This model has been considered previously in KMC studies applied to surface diffusion of clusters [32,33], and also in the same context as in the present paper [31]. The activation barriers are obtained simply by considering the crossing of two of such harmonic potentials displaced a lattice-constant unit. A more detailed description of this harmonic model can be found in Refs. [31–33]. Here we shall restrict ourselves to give the final expression for the activation energy, namely,

$$E_{ini\to fin}^{act} = \frac{\epsilon}{2}\left(\frac{E_{fin} - E_{ini}}{\epsilon} + \frac{1}{2}\right)^2, \tag{6}$$

where E_{ini} and E_{fin} are the energies of the initial and final states, respectively. Also, we called $\epsilon = ka^2$, where k is the force constant of the harmonic wells and a is the lattice constant. Throughout this work, we have taken $a = 0.3$ nm, $E_b = -0.1$ eV, and $\epsilon = 1$ eV. By performing a simple replacement in the Hamiltonian (4), the energy difference $E_{fin} - E_{ini}$ can be expressed in terms of the variation of the number of occupied neighbors (Δn) caused by a diffusing particle, i.e., $E_{fin} - E_{ini} = E_b \Delta n$.

(2) EINI: Here activation energies only depend on the energy of the initial state $E^{act} = -E_{ini}$, irrespective of the final state. In spite of its simplicity, this model has frequently been considered in the literature, in contexts similar to that of the present paper [39–41].

(3) EINI-C: This model is a slight variation of the EINI model, since it has only an additional constraint. In fact, activation energies in the EINI-C model are obtained in the same way as in the EINI model, except for the case in which the particle trying to perform the movement attempts to make a transition from a state with a nonzero coordination number ($z \neq 0$) to a state with $z = 0$. Here, these kinds of transitions are forbidden. Thus, while particles can eventually detach from a given cluster in a single diffusion event in the EINI model, this can no longer occur in the EINI-C model. Nevertheless, it is important to notice that, even in the EINI-C model, a given particle with coordination number $z = 1$ can become uncoordinated ($z = 0$) if its unique nearest neighbor moves away from it, in a licit diffusion event.

(4) EAM-Ni and EAM-Cu: With these acronyms we refer to models in which the activation energies for all possible transitions (to first-neighbor paths) in two-dimensional triangular lattices are obtained by means of the embedded atom model (EAM) [42–45]. Activation energies for nickel (EAM-Ni) and copper (EAM-Cu) employed in this paper correspond to results that have previously been reported [46].

It is worth mentioning that even by starting from a single-cluster configuration, one has a rich scenario of possible kinetic evolution. In fact, particles can evaporate from the cluster, voids can appear, and new clusters, unconnected to the original one, can also grow during the dynamic evolution process, etc. In this way, certain programming effort is necessary in order to distinguish between the main cluster (connected to the bottom of the system by a path of nearest neighbors) and other clusters in the system. Let h_i be the position of the highest occupied site at the ith column on the main cluster. We characterize the fluctuations of the interface by means of a standard estimator, such as the interface roughness $[W(L_x,t)]$, given by

$$W(L_x,t) = \sqrt{\frac{1}{L_x}\sum_{i=1}^{L_x}[h_i(t) - \bar{h}(t)]^2}, \tag{7}$$

where $\bar{h}(t) = 1/L_x \Sigma_{i=1}^{L_x} h_i(t)$.

In the following sections we present numerical results obtained by means of simulations of the KMC model and for two different kinds of initial conditions, namely, sinelike patterns and rectangular patterns, respectively. It is worth noticing that some results are presented by using nanometers (nm) as length unit, while in other cases the use of lattice units is more convenient. In any case, it is a trivial task to switch between units: for lengths along the x axis one has to multiply the length in lattice units times the distance among closest neighbors in the triangular lattice a, which was taken as $a = 0.3$ nm for models MARM, ENI, and EINI-C, while the value of a for models EAM-Ni and EAM-Cu was obtained from the lattice units of their corresponding fcc structures. For distances along the y axis an additional factor $\frac{\sqrt{3}}{2}$ appears due to the geometry of the triangular lattice.

III. KINETIC PROPERTIES IN THE DECAY OF SMALL-AMPLITUDE SINUSOIDAL PATTERNS

While according to Eq. (2) the linear continuous theory of surface diffusion predicts a vanishing asymptotic interface roughness, discrete models such as the KMC models studied in this paper often have a nonvanishing asymptotic interface roughness W_∞ at nonzero temperatures, as a consequence of the internal noise that is always present in discrete systems [47]. Thus, we propose a direct generalization of the linear continuous theory's result, in order to take into account the discrete nature of matter, regarding the prediction for the interface roughness evolution of a small-amplitude Fourier mode $A \sin(kx)$, given by

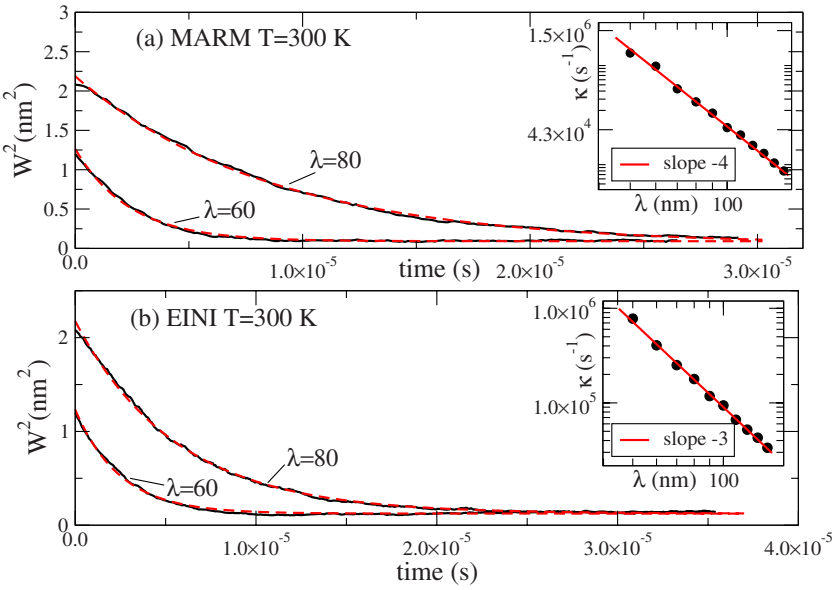

FIG. 2. (Color online) Decay of W^2 as a function of time for models MARM (above) and EINI (below). Data obtained for $T=300$ K and two different values of λ given in lattice units. The dashed lines correspond to the best fits of the data obtained by using the displaced-exponential family of functions given by Eq. (8). In the insets, the decay constants are plotted as functions of λ, showing a clear power-law dependence, with an exponent 4 in the case of the model MARM (above) and an exponent 3 for the EINI model (below).

$$W^2(\lambda,t) = \frac{A^2}{2}\exp(-2Kk^4t) + W_\infty^2[1-\exp(-2Kk^4t)]. \quad (8)$$

Figure 2 shows the temporal evolution of W^2 for the models MARM (above) and EINI (below) for different values of λ at $T=300$ K. It is found that all the curves can be fitted very well with displaced-exponential functions. Nevertheless, the insets in Fig. 2 show that although the MARM model exhibits a power-law dependence of the decay constant $\kappa \sim \lambda^{-4}$, in complete agreement with Eq. (8), the exponent becomes 3 in the case of the EINI model. Of course, it is also possible to perform a rescaling of the axes in Fig. 2 in order to obtain data collapse of the curves corresponding to different values of λ. Nevertheless, due to the different exponents governing the power-law decay of κ with λ, by rescaling a single axis one cannot achieve data collapse for both MARM and EINI models simultaneously. So, that rescaling must be done independently. However, by rewriting Eq. (8) as

$$W^2(\lambda,t) = W^2(0)\exp(-2Kk^nt) + W_\infty^2[1-\exp(-2Kk^nt)], \quad (9)$$

for an arbitrary exponent n, it becomes evident that we will be able to get data collapse after rearranging Eq. (9) as follows:

$$\frac{W^2(\lambda,t)-W_\infty^2}{W^2(0)-W_\infty^2} = \exp(-2Kk^nt). \quad (10)$$

By applying this procedure we obtained a quite good data collapse for the EINI model at 300 K, as shown in Fig. 3.

Although the generalization of the linear theory of surface diffusion provided by Eq. (8) shows good agreement with KMC data for both the MARM and EINI models, this is not the case for the models EINI-C, EAM-Ni, and EAM-Cu. For these models, a qualitatively different temporal evolution of the roughness was found: an initial linear decay of W^2 is followed, after a narrow crossover region, by an exponential decay. A typical curve for this kind of "anomalous" roughness evolution is shown in Fig. 4. The plotted data correspond to a KMC simulation for the EAM-Ni model, and the best-fit curves for the initial (linear) and final (exponential) stages are also plotted. It is clear from Fig. 4 that this transition from a linear to an exponential decaying regime takes place in a very narrow crossover region, where both curves and numerical data merge smoothly together (see the double arrow in Fig. 4).

We also studied the dependence of the lifetime τ_m of the linear regime [48] for the models EINI, EAM-Ni, and EAM-Cu corresponding to the decay of initially sinusoidal profiles with wavelengths ranging between 50 and 150 lattice units and a fixed aspect ratio equal to 0.1. In all cases, lifetime dependence on the wavelength for these models follows a power-law behavior $\tau_m \propto \lambda^\alpha$, as shown in Fig. 5. Nevertheless, the corresponding value of α varies from case to case. In fact, one has $\alpha \sim 4$ for the EAM-Cu model, while α

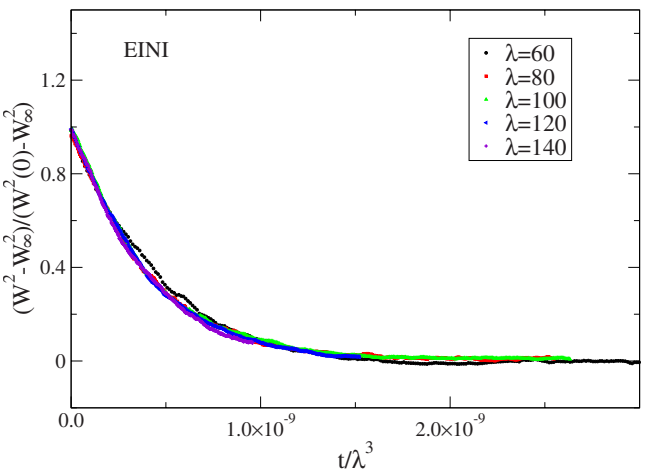

FIG. 3. (Color online) Data collapse found for results corresponding to the model EINI when the squared roughness and the time axis are rescaled as is indicated in Eq. (10). Different λ values are indicated in lattice units and the simulation temperature was 300 K.

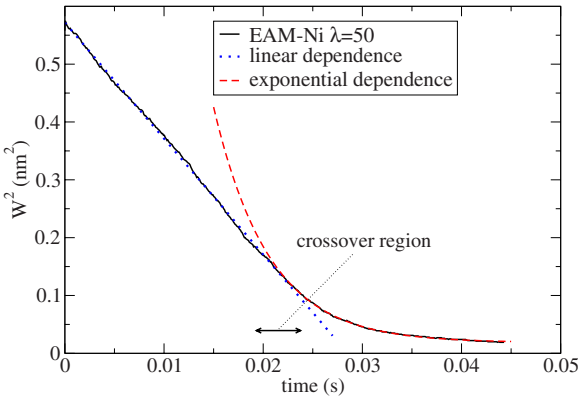

FIG. 4. (Color online) Typical behavior found for the decay of W^2 as a function of time, in the case of the EAM-Ni model (actually, the same kind of behavior is also found for models EAM-Cu and EINI-C). A transition from a linear dependence to an exponential decay is clearly observed, and the transition takes place at a narrow crossover region. The parameters corresponding to this simulation are $\lambda=50$ (in lattice units), $T=800$ K, and simulation data are averaged over 50 independent runs.

~ 4.5 for the EAM-Ni model. Moreover, in the case of the EINI-C model we found that α varies with temperature, since the computed values are $\alpha \sim 3$ at 1000 K and $\alpha \sim 3.4$ at 300 K [49].

It should be noticed that the differences between the values of α found for the EINI-C model at 300 and 1000 K are not surprising, since the actual evolution of the patterns is very different in both cases. In fact, Fig. 6 shows snapshots corresponding to the evolution of the system at these temperatures obtained, in both cases, by starting from the same initial sinusoidal profile. From the nanostructural point of view, the system evolves quite differently when temperature varies: while at low temperatures the pattern maintains a compact shape, at high temperatures a large number of vacancies and holes appear, which modifies the corresponding kinetic properties of the decaying process.

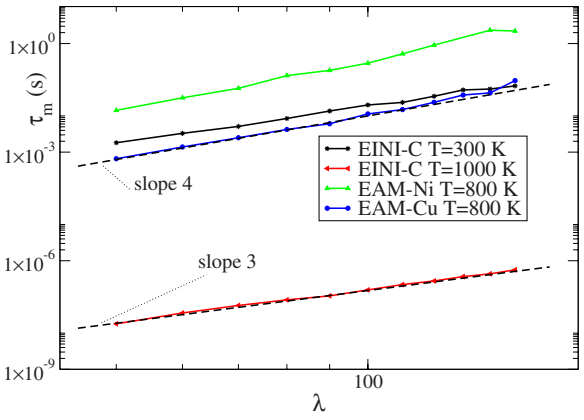

FIG. 5. (Color online) Log-log plot of the lifetime τ_m as a function of the wavelength λ (in lattice units) for models EAM-Ni, EAM-Cu, and EINI-C. In all cases this dependence is well described by a power law $\tau_m=\lambda^{\alpha}$, although the corresponding value of α varies from case to case: It is $\alpha \sim 4$ for the EAM-Cu model at $T=800$ K, $\alpha \sim 3$ for the ENI-C at $T=1000$ K, while the exponents are $\alpha \sim 4.5$ and $\alpha \sim 3.4$ for models EAM-Ni at 800 K and ENI-C at 300 K, respectively.

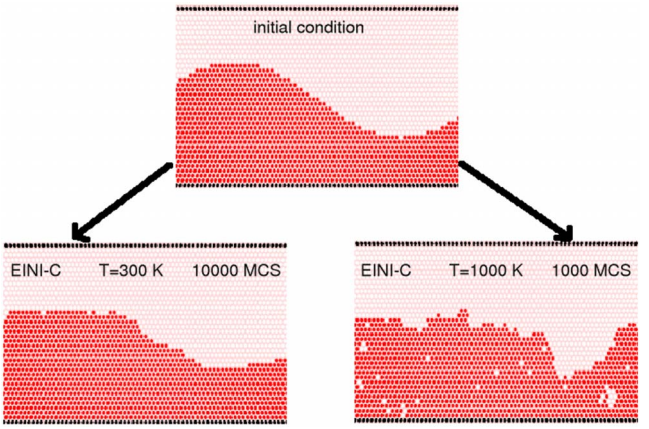

FIG. 6. (Color online) EINI-C model evolving at two different temperatures starting from the same initial condition (shown at the top). For $T=1000$ K (at the bottom on the right-hand side) one observes an important generation of vacancies and holes when compared to the evolution measured at $T=300$ K (at the bottom on the left-hand side), where neither vacancies nor holes are observed. Monte Carlo steps (MCS) corresponding to each snapshot are indicated.

IV. MORPHOLOGICAL PROPERTIES IN THE EVOLUTION OF HIGH ASPECT-RATIO NANOSTRUCTURES

So far, we have shown results of simulations focused on the decaying of sinusoidal interfaces under the small-slope approximation. In this section we present results associated with a broader class of interfaces such as rectangular patterns and high-amplitude sinusoidal interfaces. We shall discuss the morphological properties of these interfaces during their dynamic evolution and, in particular, how they are related to the dynamic evolution predicted by the continuous approach [30,31]. Geometrical parameters of the considered rectangular patterns are established in the following way: let B_s and B_i be the upper and lower bases of the pattern, and H the rectangle height (the spatial period of the pattern then is B_s+B_i). Here we are specifically interested in the relaxation behavior of patterns in the large-slope case (i.e., for $H \geqslant B_s$, B_i).

Figure 7 shows snapshots of the evolution of the different models obtained by starting, in all cases, from the same initial high-amplitude sinusoidal profile [Fig. 7(a)]. The corresponding number of MCS elapsed in each case is indicated inside the snapshots, while the temperatures are indicated in the caption of Fig. 7. A remarkable result that follows after inspection of these snapshots is the fact that, irrespective of the considered model, all are very similar and their shapes closely resemble the predictions of the continuous theory of surface diffusion in the (nonlinear) case of high amplitudes. As was discussed in Sec. I, these kinds of shapes [sketched in Fig. 1(b)] are well described by the ansatz of Eq. (3).

Focusing our attention on the evolution of initial rectangular profiles with $B_i=B_s$, we also found that the morpho-

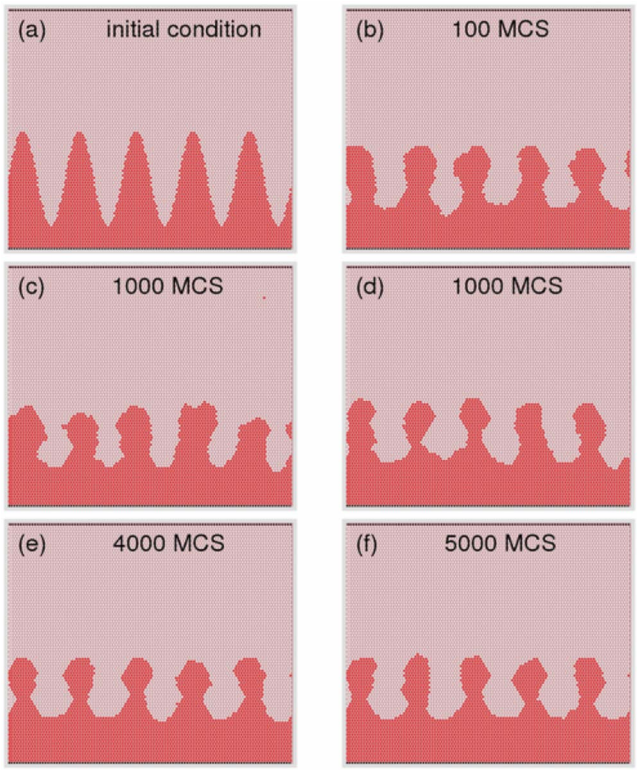

FIG. 7. (Color online) Evolution of the different models starting from the same initial sinelike profile (a) after a number of MCS indicated in each snapshot. (b) Model MARM at $T=300$ K. (c) Model EINI at $T=300$ K. (d) Model EINI-C at $T=300$ K. (e) Model EAM-Ni at $T=800$ K. (f) Model EAM-Cu at $T=800$ K. The initial profile has a wavelength $\lambda=20$ and an amplitude $A=20$ (both in lattice units), which implies an initial aspect ratio far from the small-slope approximation.

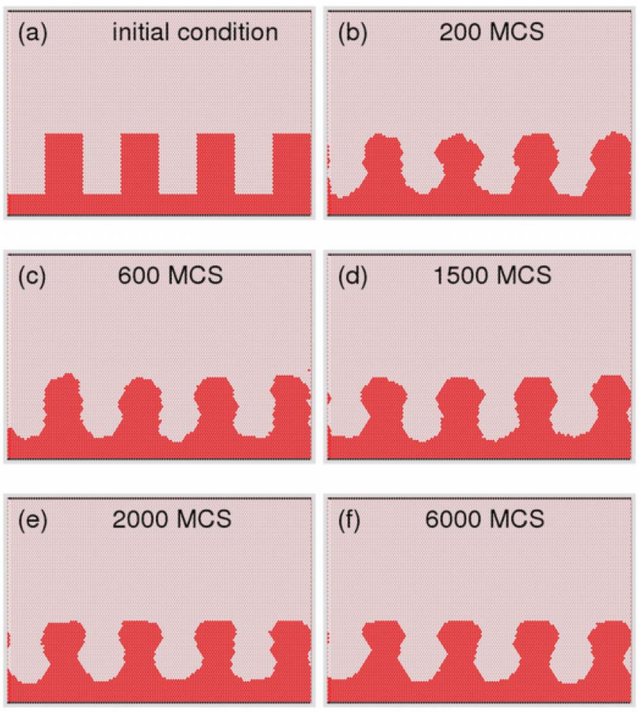

FIG. 8. (Color online) System evolution for each model considered starting from the same initial rectangular profile shown in (a), after the number of MCS indicated in each snapshot. (b) Model MARM at $T=300$ K. (c) Model EINI at $T=300$ K. (d) Model EINI-C at $T=300$ K. (e) Model EAM-Ni at $T=800$ K. (f) Model EAM-Cu at $T=800$ K. The geometrical parameters of the initial rectangular pattern are $B_i=15$, $B_s=15$, and $H=30$, all of them measured in lattice units.

logical structures formed are very similar, independently of the activation energy model considered. Furthermore, as is shown in Fig. 8, for all the models we also found that an initially rectangular profile develops patterns that are very similar to those shown in Figs. 7(b)–7(e). This finding means that in all cases a fast filtering of high-frequency modes operates, so that "memory" effects on the initial rectangular profile are lost and the systems evolve in the same way as if they were started from a sinusoidal (lowest frequency Fourier mode) profile. As was pointed out in Ref. [31], it is interesting to notice that such high-frequency filtering takes place under a clearly nonlinear regime, in which superposition-principle ideas are *a priori* no longer applicable. Of course, the snapshots of Fig. 8 were taken at different MCS, which is understable since, as we have discussed in the preceding section, kinetic properties strongly depend not only on temperature but also on the model considered for activation energies.

When $B_s \ll B_i \leqslant H$, i.e., in the case of very narrow slabs, the morphological evolution departs considerably from the case depicted in Fig. 8. In fact, Fig. 9 shows that in this case the slabs break down into several nanoislands, constituted by small isolated clusters of particles. Of course, the snapshots are taken during a metastable transient state, and after a certain time the system will evolve into a single structure by lowering its energy. Here again, Fig. 9 shows that this metastable state is observed in all cases, independently of the particular activation energy model. Although the number and size of nanoislands depend, of course, on kinetic properties (then they are also dependent on the specific model), from the morphological point of view the obtained results are qualitatively similar for all considered cases.

V. SUMMARY AND CONCLUDING REMARKS

We performed kinetic Monte Carlo simulations of two-dimensional models for the study of nanostructure decay. Different alternatives for the activation energies associated with diffusion paths, including a harmonic model (MARM), models only sensitive to the energy of the initial state of the diffusing particle (EINI and EINI-C), and also models where activation energies were obtained by means of the embedded atom model (EAM-Ni and EAM-Cu) have been considered. We addressed the study of both kinetic properties of the decay of sinusoidal profiles within the small-slope approximation, and morphological properties related to the decay of high aspect-ratio structures. The results are compared not only among the different activation energy models used, but also with the predictions from the continuous theory of surface diffusion-driven interfaces.

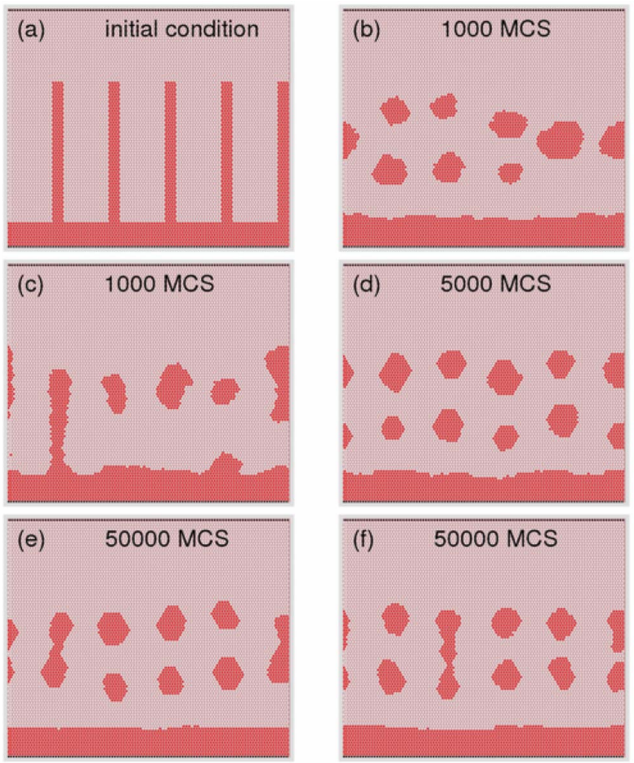

FIG. 9. (Color online) Evolution of the same initial rectangular profile (a) in the case of very narrow slabs. (b) Model MARM at $T=300$ K. (c) Model EINI at $T=300$ K. (d) Model EINI-C at $T=300$ K. (e) Model EAM-Ni at $T=800$ K. (e) Model EAM-Cu at $T=800$ K. For each model, the Monte Carlo time elapsed since the initial condition is indicated. Geometrical parameters of the initial rectangular pattern are $B_i=14$, $B_s=4$, and $H=60$, all of them measured in lattice units.

Concerning the kinetic properties of the decay of small-amplitude sinelike profiles, we found that, in the case of the MARM and EINI models, the interface roughness follows a displaced-exponential dependence, which can be considered as a natural generalization of the continuous theory. Nevertheless, we also found that for the remaining models considered (i.e., EINI-C, EAM-Ni, and EAM-Cu) the interface roughness follows a qualitatively different time decay evolution, since it is linear during an initial stage and, after a short crossover region, it becomes exponential. Although the decay-lifetime dependence on the profile wavelength follows power laws in all cases, the associated exponent is model dependent.

Concerning the morphological properties of high aspect-ratio pattern decay, we found that shape evolution is qualitatively similar irrespective of the particular activation energy model used and, even more remarkable, this evolution is quite similar to that predicted by the continuous theory of surface diffusion. In particular, sinusoidal profiles of high initial amplitudes show the spontaneous development of overhangs during a transient stage, and the interface shape can approximately be described by the ansatz given by Eq. (3). Moreover, for the decay of rectangular patterns of height H, and upper and lower bases B_s, and B_i, respectively, we found that, for $B_s \sim B_i \sim H$, the evolution proceeds rapidly filtering high-frequency spatial modes and then, after a short transient, the interface profile is nearly the same as if the initial profile were a sinelike one. In the case of very narrow rectangular slabs ($B_s \ll B_i \leqslant H$), rectangles break down into several nanoislands during a transient regime. Although the number and size of such nanoislands depend on kinetic aspects, such as the particular activation energy model, from a morphological point of view, we found that this transient regime is observed in all cases and it looks qualitatively similar irrespective of the activation energy model considered.

In short, from this work we conclude that kinetic properties of nanopattern decay strongly depend on the activation energy model considered. In this sense, kinetic predictions from the continuous theory of surface diffusion are expected to be in agreement with the observation of the actual evolution of a discrete system, only in some particular cases. In contrast, continuous theory predictions concerning morphological aspects show a wider applicability. In fact, that theory describes, in a qualitatively correct way, the observed morphologies in a wide range of situations and irrespective of the activation energy model considered. In this way, we expect that this work will contribute to stimulate experimental research in this field aimed to test, in real nanotechnological systems, the predictions of the continuous surface diffusion theory concerning morphological aspects. Thus, by identifying the correct model capable of describing an actual physical system, computer simulations can become a powerful tool aiding the nonexpensive design of nanodevices and nanopatterns.

ACKNOWLEDGMENTS

This work has been performed as part of the projects PICT 06-621 and PICT 06-36 of ANPCyT (Argentina). The authors acknowledge of CONICET (Argentina National Research Council) and UNLP.

[1] G. S. Bales, A. C. Redfield, and A. Zangwill, Phys. Rev. Lett. **62**, 776 (1989).
[2] R. P. U. Karunasiri, R. Bruinsma, and J. Rudnick, Phys. Rev. Lett. **62**, 788 (1989).
[3] N. Israeli and D. Kandel, Phys. Rev. Lett. **80**, 3300 (1998).
[4] H. Kallabis and D. E. Wolf, Phys. Rev. Lett. **79**, 4854 (1997).
[5] E. S. Fu, M. D. Johnson, D. J. Liu, J. D. Weeks, and E. D. Williams, Phys. Rev. Lett. **77**, 1091 (1996).
[6] J. Erlebacher, M. J. Aziz, E. Chason, M. B. Sinclair, and J. A. Floro, Phys. Rev. Lett. **84**, 5800 (2000).
[7] M. A. Dubson and G. Jeffers, Phys. Rev. B **49**, 8347 (1994).
[8] A. Maritan, F. Toigo, J. Koplik, and J. R. Banavar, Phys. Rev.

Lett. **69**, 3193 (1992).
[9] C.-S. Son, T. Kim, X.-L. Wang, and M. Ogura, J. Cryst. Growth **221**, 201 (2000).
[10] M. V. Ramana Murty, Phys. Rev. B **62**, 17004 (2000).
[11] N. Israeli and D. Kandel, Phys. Rev. Lett. **88**, 116103 (2002).
[12] H. C. Kan, S. Shah, T. T. Tadyyon-Eslami, and R. J. Phaneuf, Phys. Rev. Lett. **92**, 146101 (2004).
[13] H. P. Bonzel and E. E. Latta, Surf. Sci. **76**, 275 (1978).
[14] H. P. Bonzel and E. Preuss, Surf. Sci. **336**, 209 (1995).
[15] M. Giesen-Seibert, R. Jentjens, M. Poensgen, and H. Ibach, Phys. Rev. Lett. **71**, 3521 (1993).
[16] M. Giesen-Seibert and H. Ibach, Surf. Sci. **316**, 205 (1994).
[17] G. L. Timp, *Nanotechnology* (Springer-Verlag, New York, 1999).
[18] M. Kolb, R. Ullmann, and T. Will, Science **275**, 1097 (1997).
[19] M. Rieth, *Nano-Engineering in Science and Technology* (World Scientific, Singapore, 2003).
[20] G. Andreasen, P. L. Schilardi, O. Azzaroni, and R. C. Salvarezza, Langmuir **18**, 10430 (2002).
[21] W. W. Mullins, J. Appl. Phys. **28**, 333 (1957).
[22] W. W. Mullins, J. Appl. Phys. **30**, 77 (1959).
[23] C. Herring, in *Physics of Powder Metallurgy*, edited by W. E. Kingston (McGraw-Hill Book Company, Inc., New York, 1951).
[24] C. Herring, in *Structure and Properties of Solid Surfaces*, edited by R. Gomer and C. S. Smith (The University of Chicago Press, Chicago, 1952).
[25] J. Lapujoulade, Surf. Sci. Rep. **20**, 191 (1994).
[26] D. E. Wolf and J. Villain, Europhys. Lett. **13**, 389 (1990).
[27] S. Das Sarma and P. Tamborenea, Phys. Rev. Lett. **66**, 325 (1991).
[28] A. L. Barabasi and H. E. Stanley, *Fractal Concepts in Surface Growth* (Cambridge University Press, Cambridge, 1995).
[29] M. F. Castez, M. H. Fonticelli, O. Azzaroni, R. C. Salvarezza, and H. G. Solari, Appl. Phys. Lett. **87**, 123104 (2005).
[30] M. F. Castez, R. C. Salvarezza, and H. G. Solari, Phys. Rev. E **73**, 011607 (2006).
[31] M. F. Castez and E. V. Albano, J. Phys. Chem. C **111**, 4606 (2007).
[32] H. C. Kang and W. H. Weinberg, Phys. Rev. B **38**, 11543 (1988).
[33] H. C. Kang and W. H. Weinberg, J. Chem. Phys. **90**, 2824 (1989).
[34] K. A. Fichthorn and W. H. Weinberg, J. Chem. Phys. **95**, 1090 (1991).
[35] N. Metropolis, A. W. Rosenbluth, M. N. Rosenbluth, A. H. Teller, and E. Teller, J. Chem. Phys. **21**, 1087 (1953).
[36] R. J. Glauber, J. Math. Phys. **4**, 294 (1963).
[37] K. Kawasaki, in *Phase Transitions and Critical Phenomena*, edited by C. Domb and M. S. Green (Academic, New York, 1972), Vol. 2.
[38] D. W. Heermann, *Computer Simulation Methods* (Springer-Verlag, Heidelberg, 1989).
[39] N. Combe, P. Jensen, and A. Pimpinelli, Phys. Rev. Lett. **85**, 110 (2000).
[40] N. Combe and H. Larralde, Phys. Rev. B **62**, 16074 (2000).
[41] J. L. Iguain and L. J. Lewis, Phys. Rev. B **68**, 195407 (2003).
[42] M. S. Daw and M. I. Baskes, Phys. Rev. Lett. **50**, 1285 (1983).
[43] M. S. Daw and M. I. Baskes, Phys. Rev. B **29**, 6443 (1984).
[44] R. A. Johnson, Phys. Rev. B **37**, 3924 (1988).
[45] Y. G. Yang, R. A. Johnson, and H. N. G. Wadley, Acta Mater. **45**, 1455 (1997).
[46] Y. Yang, Ph.D. thesis, University of Virginia, 2000 (unpublished).
[47] N. G. V. Kampen, *Stochastic Processes in Physics and Chemistry* (Elsevier Science B. V., Amsterdam, The Netherlands, 1992).
[48] The lifetime was computed as $\tau_m = -\frac{B}{2m}$, where m is the slope and B is the ordinate at the origin of the corresponding linear equation.
[49] Reported values of α are very approximated, since they were obtained with rather low statistics, particularly in the case of large wavelengths.